Understanding Molecular Motor Walking along a Microtubule: A Themosensitive Asymmetric Brownian Motor Driven by Bubble Formation

Noriyoshi Arai,*[,†,‡,¶] Kenji Yasuoka,[‡] Takahiro Koishi,[§] Toshikazu Ebisuzaki,[¶] and Xiao Cheng Zeng[∥]

[†]Department of Mechanical Engineering and Intelligent Systems, University of Electro-Communications, Chofu, Tokyo, Japan
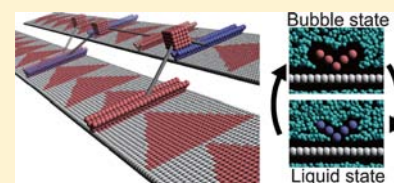[‡]Department of Mechanical Engineering, Keio University, Yokohama, Japan
[¶]Computational Astrophysics Laboratory, RIKEN, Wako, Saitama, Japan
[§]Department of Applied Physics, University of Fukui, Fukui, Japan
[∥]Department of Chemistry, University of Nebraska—Lincoln, Lincoln, Nebraska, United States

Ⓢ Supporting Information

ABSTRACT: The "asymmetric Brownian ratchet model", a variation of Feynman's ratchet and pawl system, is invoked to understand the kinesin walking behavior along a microtubule. The model system, consisting of a motor and a rail, can exhibit two distinct binding states, namely, the random Brownian state and the asymmetric potential state. When the system is transformed back and forth between the two states, the motor can be driven to "walk" in one direction. Previously, we suggested a fundamental mechanism, that is, bubble formation in a nanosized channel surrounded by hydrophobic atoms, to explain the transition between the two states. In this study, we propose a more realistic and viable switching method in our computer simulation of molecular motor walking. Specifically, we propose a thermosensitive polymer model with which the transition between the two states can be controlled by temperature pulses. Based on this new motor system, the stepping size and stepping time of the motor can be recorded. Remarkably, the "walking" behavior observed in the newly proposed model resembles that of the realistic motor protein. The bubble formation based motor not only can be highly efficient but also offers new insights into the physical mechanism of realistic biomolecule motors.

INTRODUCTION

Feynman proposed the ratchet and pawl device in 1963[1] as a model of biological motors. This device, utilizing two heat reservoirs with different temperatures, can produce single-direction motion from random Brownian fluctuations. The theoretical concept of the Feynman's ratchet and pawl device has been extended to a more generalized model involving Brownian particles placed in an asymmetric periodic potential, and such a mode has been linked to the operation of nanomotors in biological systems.[2−7] More specifically, the model consists of a motor particle and a rail that can exhibit two binding states: "the random Brownian state" and "the asymmetric potential state". In the random Brownian state, the particle undergoes one-dimensional random walking movement along the rail. In the asymmetric potential state, the motor particle is subject to an asymmetric potential of sawtooth shape from the rail, besides the random forces from ambient molecules. As the system changes its state from the Brownian to asymmetric and *vice versa*, the motor particle moves stochastically but overall in a single direction. The probability of forward movement is higher than backward movement due to the asymmetric potential.[8,9] Moreover, the motor particle moves in a stepwise manner, with each step corresponding to the unit length of the periodic structure of the rail which gives rise to the asymmetric potential.

It is well-known that a single KIF1A monomer, that is, the simplest biological motor protein, displays a similar single-direction "walking" behavior along a microtubule.[10−12] For example, the KIF1A monomer shows stepwise motion of 8-nm units, which correspond to the repeating pattern of the micro-tubule.[13,14] The KIF1A monomer also shows a biased displacement through biased binding to the microtubule. Similar behaviors of single-direction motion have been observed in muscle contraction produced by the actin−myosin system.[15]

In our previous study, we proposed a fundamental "switch" mechanism between the two states, namely, the bubble formation in a nanosized channel surrounded by hydrophobic atoms.[16] In that model, the system consists of a small board (the motor) with hydrophobic surfaces and a nanorail, which entails left−right asymmetric patterns of hydrophobic molecules. The bubble formation is controlled by changing the channel distance between the motor and the rail by an atomic distance (∼0.1 nm). When the motor is close to the rail, water molecules between them are expelled out of the narrow channel. A bubble or cavity forms due to the stronger hydrophobic effect. The motor is subject to the asymmetric potential and is captured by the potential well. On the other hand, when the motor is not close to

the rail, the narrow channel is filled with the water molecules. The motor fluctuates thermally and can move randomly along the rail. We referred to the former state as the "bubble state", and the latter state as the "liquid state". The bubble and liquid states correspond to strong and weak binding (of motor) states, respectively. Behaviors of the model motor observed in the simulation seem in good agreement with actual motor proteins. In our previous model,[16] the height of the motor is controlled by an external force, which mimics the conformational change during ATP hydrolysis. We also found that a fine-tuning in the temporal profile and strength of the external force are necessary to render the system as an efficient motor, like nanosized biomotors. Such a fine-tuning is unlikely to occur in biological systems.

To overcome this difficulty, in the present paper, we propose a much improved model, in which the hydrophobic/hydrophilic parameter of a motor is controlled by the temperature of the motor itself. An example of such a moter is the thermosensitive polymers, which exhibit phase transition between hydrophobic and hydrophilic states. It has been recently reported that poly(*N*-isopropylacrylamide), which can be planted on the solid surface, can change its conformation with temperature. As a result, drastic change in the surface hydrophobicity can be realized.[17,18] Since the transition between hydrophobic and hydrophilic states occurs at the critical temperature of ∼307 K, which is close to in vivo temperature, such a hydrophobicity/hydrophilicity change may play an important role in biological systems. Motivated by the finding of this novel property of the thermosensitive polymer, we propose to devise a bubble-formation motor system that can be controlled by temperature pulses.

The following section elucidates the methodology for constructing a bubble-formation motor system by controlling temperature of the motor. A comparison of this system to experimental data of the KIF1A motor protein is given. Furthermore, we construct a double-headed motor system (see below) for the modeling of kinesin or myosin. Motion behavior of the double-headed motor system is simulated under a constant force.

■ SIMULATION METHODS AND MODEL SYSTEM

We employ the dissipative particle dynamics[19−21] (DPD) simulation method, which is a powerful mesoscopic tool that enables simulation of events occurring within the millisecond time scale and the micrometer length scale. A DPD particle represents coarse-grained atoms or molecules that are subject to three types of forces: conservative, dissipative, and random. The motion of the particles obeys Newton's laws. Details of the force formula and interaction parameters have been given elsewhere.[16] Since the introduction of the DPD method a decade ago, it has been applied to a variety of different complex fluid systems, such as penetration of nanoparticles into a lipid bilayer,[22] self-assembly of surfactants,[23,24] and DNA controlled assembly.[25,26]

We construct two systems, the single-headed (Figure 1) system and the double-headed motor system. The former includes a motor and a rail, while the latter includes two motors, two rails, and a neck linker. The double-headed motor system is explained in more detail later. In the single-headed motor system, both the motor (Figure 1a) and the rail (Figure 1b) are immersed in water (Figure 1c), and both are treated as rigid bodies. The motor is a V-shaped nanobar, allowing inflow and outflow of water molecules from the narrow channel between the nanobar and the rail once hydrophobicity of the motor is altered. The rail is composed of strongly (red) and weakly (white) hydrophobic particles.
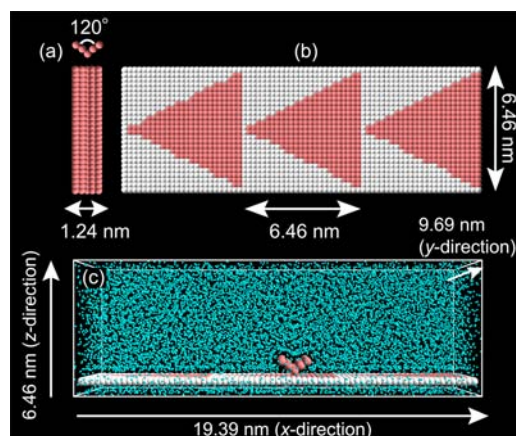

Figure 1. The motor system is composed of a motor and rail. (a) The motor is a V-shaped nanobar made of dissipative beads. The hydrophobicity/hydrophilicity of the motor can be switched back and forth, depending on the instant temperature of the motor. (b) The rail is made of both strongly (red) and weakly (white) hydrophobic beads. The pattern of the strongly hydrophobic beads is left−right asymmetric, in this case, given by triangles. (c) A side (perspective) view of the motor system. The motor (red) and rail (red and white) are immersed in water (cyan).

In our DPD simulations, the cutoff radius of the DPD parameter, r_c, is ∼0.646 nm. We have adopted the method by Groot and Rabone for scaling of length and time.[27] We used 15 580 particles in the single motor system. The number of water, rail, and motor particles were 13 500, 1950, and 130, respectively. Also, for the kinesin model (double-headed) motor system, a neck linker, a motor, and a rail are added to the single motor system. The neck linker is cubic and composed of 125 particles. Therefore, the total number of particles is 31 285. The simulation box size is 19.39 × 9.69 × 6.46 nm³ in single-headed motor system and 19.39 × 19.39 × 6.46 nm³ in the double-headed model motor system. The periodic boundary conditions are applied in all directions. All simulations are carried out in the canonical ensembles using a modified velocity-Verlet integration algorithm with a time step of $\Delta t = 1.76$ ps. In the DPD simulation, the system temperature is controlled by balancing the random and dissipative forces such that the fluctuation-dissipative theorem is met.

For the single-head motor system, an average lifetime, τ, in the hydrophobic state is set to 17.6 ns. We switch the hydrophobic state of the motor once the probability $P^* = \exp[\tau/(t - t_i)]$ is smaller than a random number generated uniformly in every step. Here, t_i is a time when the switching event occurs. Also we set the critical temperature for transition between the hydrophobic state and hydrophilic state, $T_c \approx 1.1 k_B T$. Here, k_B is the Boltzmann constant. In our simulation, the motor is in the hydrophobic state at a temperature ($1.0 k_B T$) below the T_c, and it changes to the hydrophilic state above the T_c. The temperature of the motor, T_m, is estimated by $(2M_m/f)((dX_m/dt)^2 + (dZ_m/dt)^2)^{1/2}$ where f is the number of degrees of freedom. By using velocity scaling on the motor molecules, T_m can be increased above the critical temperature in simulations. The preset temperature, T_s, alternates between $1.2 k_B T$ and $1.0 k_B T$ in the simulations. For $T_s = 1.2 k_B T$, T_m is controlled at T_s through a scaling factor $(T_s/T_m)^{1/2}$. By this manipulation, the chemical nature of the motor becomes instantly hydrophilic. We apply the velocity scaling in every time step while the motor is in the hydrophilic state. Also, the input energy, E_{in}, is defined as the energy used for

the increasing temperature in order to set the motor in the hydrophilic state. By contrast, for $T_s = 1.0k_BT$, the motor exchanges the momentum with surrounding water particles in the simulation. As a result, the momentum of the motor dissipates within a short period, and T_m converges to $1.0k_BT$ without any artificial input energy. Note that the system temperature is $1.0k_BT$ all the time in all simulations, but T_m is $1.2k_BT$ in the hydrophilic state. This higher local temperature is achieved by applying the velocity scaling method to the motor only, and it has little influence on the system temperature since the number of particles that constitute the motor is far less than the number of water particles in the system.

When the motor is in the hydrophobic state, interaction parameters for motor/strong hydrophobic rail, motor/weak hydrophobic rail, and motor/water pairs are $25k_BT$, $50k_BT$, and $100k_BT$, respectively. When the motor is in the hydrophilic state, interaction parameters for motor/rail (a_{mr}) and motor/water (a_{mw}) pairs change to $a_{mr} = 100k_BT$, and $a_{mw} = 25k_BT$. In the double-headed motor model, motors are connected to the neck linker by a weakly harmonic spring with a spring constant of $0.02k_BT/r_c^2$. The mass of particles comprising the neck linker is 100 times larger than other particles. In our model, a weak electrostatic interaction is exerted so that the motor cannot detach from the rail completely in the negative z-direction. The added electrostatic interaction between the motor and the rail is time independent with the magnitude of ∼1.77 pN.

Equation of Motion in Our Motor System. Because we assume the rail, the neck linker, and the motor to be rigid, the particles in the rail, the motor, and the neck linker do not move with respect to the centers of mass. Rotational motions of the motor and the neck linker are restricted in our model. We take the center of mass of the rail as the coordinate origin.

$$\mathbf{R}_{rail} = (0, 0, 0) \tag{1}$$

The position of the motor and the neck linker are calculated by

$$M_m \frac{d^2 X_m}{dt^2} = F_{m,x}/N_m \tag{2}$$

$$M_m \frac{d^2 Z_m}{dt^2} = F_{m,z}/N_m \tag{3}$$

$$M_n \frac{d^2 X_n}{dt^2} = F_{n,x}/N_n \tag{4}$$

$$M_m \frac{d^2 Y_m}{dt^2} = M_n \frac{d^2 Y_n}{dt^2} = M_n \frac{d^2 Z_n}{dt^2} = 0 \tag{5}$$

where subscript m and n represent the motor and the neck linker, respectively. $F_x = \sum_i^N f_{x,i}$ and $F_z = \sum_i^N f_{z,i}$. M is a mass, X, Y, and Z are the position of the center of mass in the x-, y-, and z-directions, respectively. N is the number of particles that composes the motor or the neck linker. The motor only moves in the x- and z-directions, and the neck linker only moves in the x-direction.

Efficiency of Motor System. The energy efficiency, η, of the motor system can be estimated by the work required to move surrounding water molecules in the x-direction, divided by the input energy, E_{in}, required to induce phase transition:

$$\eta = \frac{\Delta t \sum_{t_s}^{t_e} \left(\sum_i^N f_{x,i} \right)(x_k - x_{k-1})}{\Delta t \sum_{t_s}^{t_e} E_{in}} \tag{6}$$

where t_s and t_e are the starting and ending time of the measurement, respectively, and $f_{x,i}$ is the conservation force exerted by the ith particle composing the motor (single-headed motor model) or the neck linker (double-headed motor model), and x_k represents the position of the motor in the single-headed motor system at the kth time-step or the position of the neck linker in the double-headed motor system.

■ RESULTS AND DISCUSSION

Stable Binding Distance for Two States. The hydrophobic/hydrophilic state of the motor can be switched back and forth, each with an average lifetime of τ (see definition in the Simulation Methods and Model System section). This switching corresponds to ATP hydrolysis. First, we estimated the natural binding states for the hydrophobic and hydrophilic motor without any external force. The simulation starts from various initial positions in the z-direction $Z_m = Z_0$ of the motor, where Z_0 is set at 1.22, 1.47, 1.73, 1.99, and 2.25 nm. Here Z_m stands for the location of the center of mass of the motor in the z-direction. The position of the motor is first restricted at Z_0 for 35.2 ns to allow surrounding water molecules equilibrate. The motor is then allowed to relax to monitor the change in Z_m, as shown in Figure 2. In the cases of hydrophobic state of the motor, Z_m converged to $Z_m \approx 1.33$ nm, and water beads are pushed out of
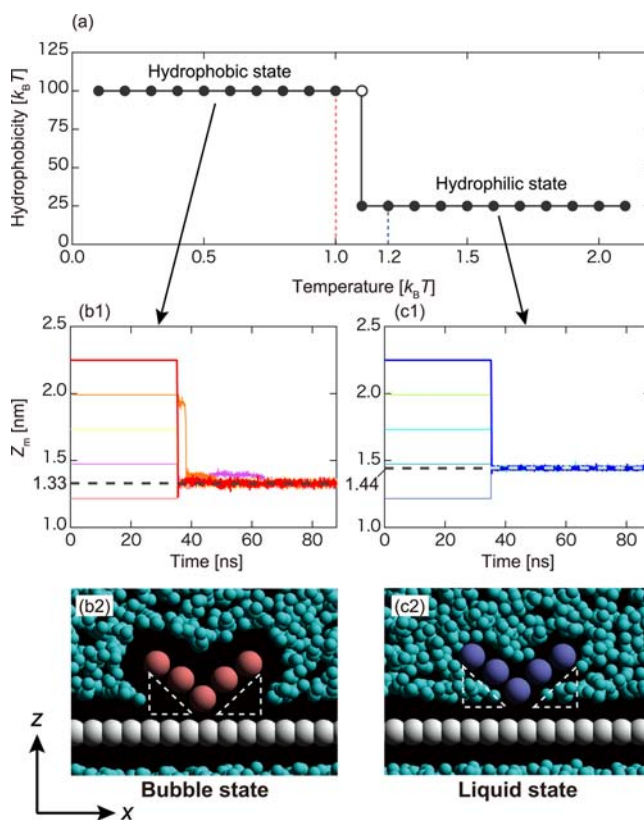

Figure 2. (a) Temperature dependence of the hydrophobicity of the motor. Here, the hydrophobic state means the maximum repulsion between the motor and the water in the conservative force of the dissipative particle method. Red and blue (vertical) dashed lines represent preset temperatures in the hydrophobic and hydrophilic states, respectively. (b1, c1) Time evolution of the distance between the motor and the rail in the z-direction. The black dashed lines are the time-averaged position of the motor. (b2, c2) Snapshots of the system around the motor (side view), where the distribution of the water is projected to the x−z plane: left, bubble state; right, liquid state.
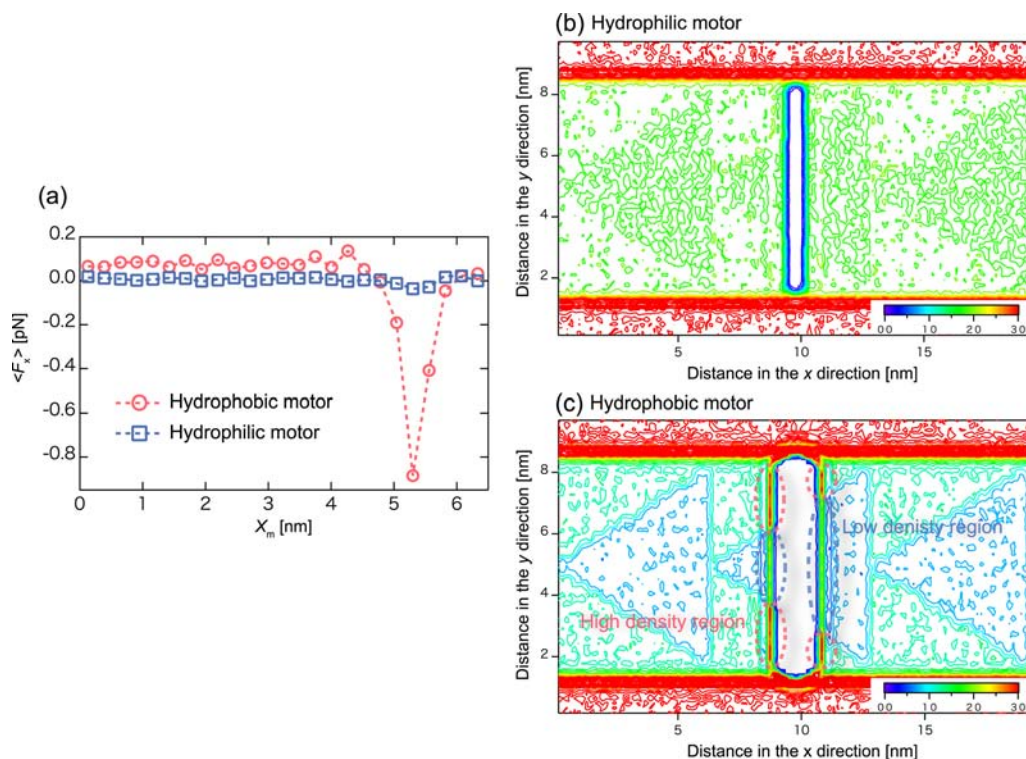
Figure 3. (a) Time -averaged force acting on the motor, $\langle F_{m,x} \rangle$, in the x-direction. The horizontal axis is the position of the motor, X_m, and shows one periodic pattern of the rail. The red circles and blue squares represent $Z_m \approx 1.33$ nm (bubble state) and $Z_m \approx 1.44$ nm (liquid state), respectively. (b) Contour line of water density around the motor with $Z_m \approx 1.44$ nm (liquid state). (c) Contour line of water density around the motor with $Z_m \approx 1.33$ nm (bubble state). Consistent with panel a, the liquid state and bubble state correspond to the random Brownian state and asymmetric potential state, respectively.

the channel between the motor and the rail (denoted by white triangles in Figure 2c). As a result, the motor system adopts the bubble state and is subject to the asymmetric potential (discussed later). In contrast, in the cases of hydrophilic state of the motor, the motor position converged into $Z_m \approx 1.44$ nm. Water beads occupy the channel (triangles in Figure 2c). As such, the motor moves randomly along the rail (discuss later). Therefore, the motor spontaneously locates a new stable position Z_m only after the hydrophobicity/hydrophilicity of the motor is changed, and concomitantly two natural bindings are established. The difference among the stable positions Z_m is very small, about 0.11 nm. Actual motor proteins also possess two binding states. The motor proteins attach and detach from the microtubule based on the two states and move processively. In our motor system, the hydrophilic motor has a higher temperature than the surrounding (ambient) water for modeling of a configuration change of a thermosensitive polymer. The hydrophobic motor can be turned into the hydrophilic one at a specific temperature. Such a change in hydrophobicity of the motor results in a change of state of the system from the bubble state to the liquid state.

Effective Potential and Contour Line of Water Density. The time-averaged force acting on the motor in the x-direction, $\langle F_{m,x} \rangle$, due to surrounding water beads in each state is computed to derive an effective potential function. In the bubble state (red circles in Figure 3a), the sign of $\langle F_{m,x} \rangle$ switches from positive to negative at $X_m \approx 4.5$ nm, beyond which the motor is subject to the asymmetric potential (in a curved sawtooth shape). In the liquid state, however, $\langle F_{m,x} \rangle$ is negligibly small (<0.04 pN) for all X_m positions (blue squares in Figure 3a). The liquid state corresponds to the random Brownian state. This result indicates that the asymmetric Brownian ratchet model can be realized

by switching the state of the motor: When in the hydrophobic state, the motor is captured into the potential well (for example, $X_m \approx 4.5$ nm in Figure 3a where the sign of $\langle F_{m,x} \rangle$ switches from positive to negative). When the motor is switched to the hydrophilic state, the potential function becomes flat. The motor can move randomly (the Brownian motion). Thereafter, the state of motor switches back to the hydrophobic state. Again, the motor is captured into the same potential well as previously if the motor moves little in the hydrophilic state. If not, the motor would move into the neighboring positive or negative potential well. As such, the motor can overcome deep potential wells from time to time by switching between the two states. Note that the motor is more likely to be captured into the positive potential well due to the difference in the potential slope.

Next, the contour lines for the density of water beads around the motor are shown in Figure 3b,c for $X_m \approx 9.69$ nm. In the case of the bubble state, a high water-density region is located around the motor. The length of the high-density region in the left-hand side is greater than that in the right-hand side due to the asymmetric hydrophobic patterns on the rail. As a result, the surrounding water molecules exert a left-to-right asymmetric pressure on the motor, and the movement of the motor is induced by the pressure difference. By contrast, in the liquid state, there is no clear density enhancement around the motor, because the bias in the force exerted on the motor is almost zero.

Motion of Motor. Figure 4 shows the time evolution of the preset temperature of the motor T_s, the input energy E_{in}, the displacement of the motor in the z-direction, Z_m, and that in the x-direction, X_m. Because the probability for the motor to move in the positive x-direction is higher than that in the negative x-direction, the motor moves forward even without a net force.
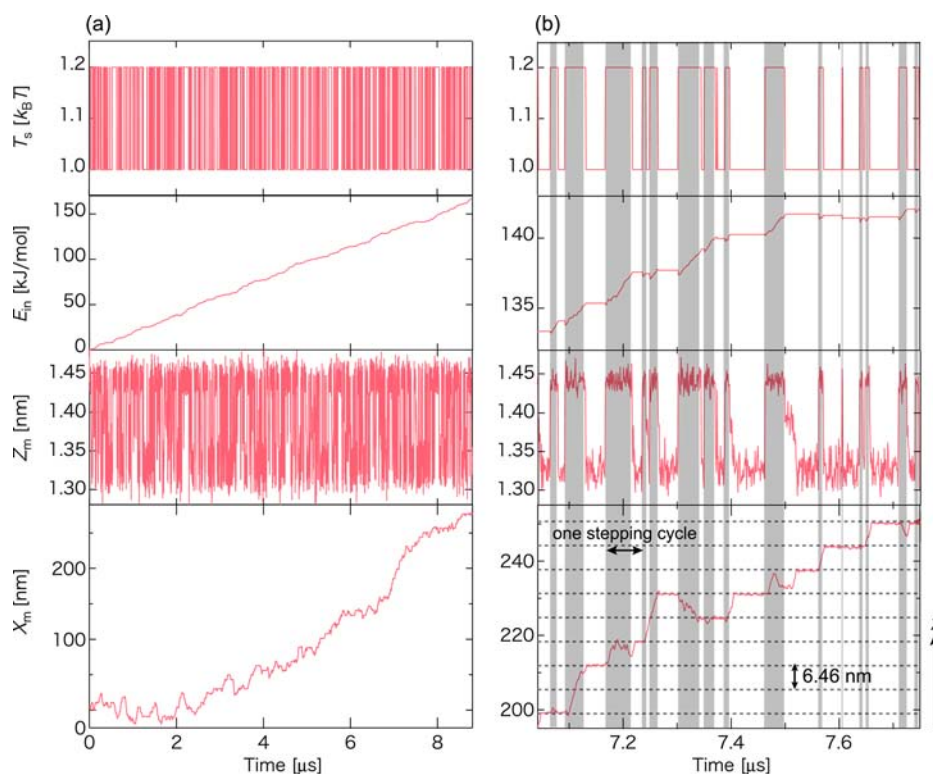
Figure 4. (a) Time evolution of a preset temperature of the motor, T_s, the input energy, E_{in}, the displacement of the motor in the z-direction, Z_m, and that in the x-direction, X_m. (b) A zoomed view of corresponding panels of part a from 7.04 to 7.75 μs. The gray areas represent the liquid state and horizontal dashed lines (bottom panel) represent periodicity of the rail structure in the x-direction. The motor fluctuates in one direction following the random Brownian motion.

Note that the net force is a potential slope for driving the motor (see ref 4 in detail). Figure 4b displays a zoomed view of Figure 4a from 7.04 to 7.75 μs. Time intervals are colored in gray when the channel between the motor and the rail is filled with water. The dashed lines in the bottom panel represent periodicity of the rail structure, which also entails asymmetric left−right patterns.

The motor moves randomly in the x-direction when the motor is not close to the rail ($Z_m \approx 1.44$ nm) because the motor is in the hydrophilic state. When the motor is the hydrophobic state, the channel between the motor and the rail becomes narrower ($Z_m \approx 1.33$ nm). The transition to the bubble state takes place. As such, the motor is subject to the asymmetric potential of rail and tends to be captured in potential wells. The bias (or the net force) is caused by the local water density difference around the motor in the x-direction (Figure 3c). The motor walks stochastically in one direction after turning on hydrophobicity of the motor, and the asymmetric Brownian model is realized in this system (movie S1, Supporting Information). The motor walks stepwise with a unit step of 6.46 nm, and this unit step corresponds exactly to the period of the triangle pattern along the rail. The motion behavior displayed in Figure 4 is similar to that of the motor protein KIF1A.[11,12] We have also estimated the energy efficiency η in this motor system (see Simulation Methods and Model System), which is about 59.8%, averaged over four simulations.

Analysis of a Single Step. In Figure 5, we display distributions of stepping size, X_{step}, and stepping time, t_{step}, for $\tau = 4.4$, 8.8, 13.2, and 17.6 ns, respectively. The stepping size is defined as the movement of the motor per one stepping cycle, and the stepping time is the duration of the stepping movement. The total count is more than 5000 stepping events. In the liquid state

(Figure 5a1), the distribution of X_{step} is Gaussian-like for all τ values (the Gaussian variance σ^2 is summarized in Table 1). Thus, the motion of the motor in the liquid state is a one-dimensional Brownian motion. On the other hand, the motor motion in the bubble state is asymmetric for all τ values. The frequency of the positive movement is higher than that of negative. From this result, we deduce that the probability of the forward step is about twice that of the backward step for $\tau = 17.6$ ns. Also, the asymmetry is obvious when τ is longer; the frequency of forward step is higher. The higher efficiency is expected with the longer τ. As can be seen in Figure 5b1,b2, t_{step} follows single-exponential distributions in both hydrophilic and hydrophobic states (slopes are summarized in Table 1). This indicates that the past history has no effect on the stepping movement. Our results are in good agreement with experimental observations.[12,28,29]

Double-Headed Motor System. In previous sections, we mainly discussed behaviors of the single-headed motor system (there is only one motor in the system). However, most realistic motor proteins, for example, kinesin and myosin, possess two motors and can also move processively. In this subsection, we focus on a double-headed motor system: One additional motor and rail are added onto the single headed motor system as shown in Figure 6. The motor and the rail are exactly the same as in the single-headed motor and are arranged to be parallel to one another (Figure 6d). In the double-headed motor system, each motor connects to the neck linker model (Figure 6a) via a harmonic spring. The neck linker only moves in the x-direction, and it is not allowed to have other translational or rotational motions. In an actual motor protein,[14,30] the motions of the motors are restricted by the linker loop. Therefore we model the
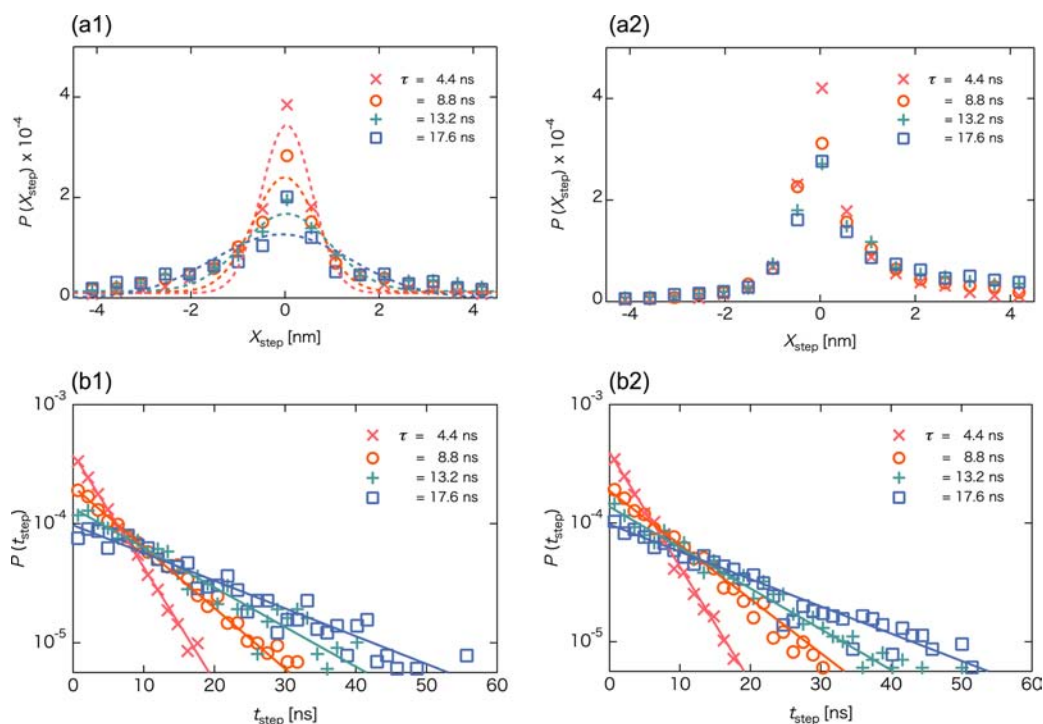
Figure 5. Stepping motion of the motor. (a) Deviation of the X_m in a single step when the motor is in the (a1) hydrophilic and (a2) hydrophobic state. Data are fitted to Gaussian curves (dashed curves). (b) Distribution of the stepping time when the motor is in the (b1) hydrophilic and (b2) hydrophobic state. The data are fitted to exponential curves (solid lines).

Table 1. Summary of the Numerical Results for Various Average Life Time, τ, Simulations

τ [ns]	σ^2	slope in liquid state	slope in bubble state
4.4	0.58	0.220	0.229
8.8	0.81	0.117	0.115
13.2	1.30	0.077	0.078
17.6	1.45	0.054	0.058

loop as the neck linker. Also, we set up the mass of particles comprising the neck linker to be greater than other particles so as to weaken the influence of the thermal fluctuation. Motors whose hydrophobicity and hydrophilicity change alternatively can walk along each rail, the same as the single-headed motor system. The switching manner occurs as follows: when the distance between motors is greater than one-half length of the asymmetric pattern on the rail (6.46 nm in our model) or, based on the average lifetime τ, when the hydrophobicities of the two motors exchange one another. The former exchange expresses a conformational change of a motor protein such as ATP/ADP bindings.

Figure 7 shows the time evolution of the preset temperature of the motor, T_s, the input energy E_{in}, the displacement in the z-direction of the motor, Z_m, the displacement in the x-direction of the motor, X_m, and that of the neck linker, X_n. Figure 7b displays an enlarged view of Figure 7a from 8.0 to 8.5 μs. Again, the gray dashed lines in the bottom panel represent the rail structure as used in the single-headed motor system (Figure 4b). Each motor is subject to the liquid and bubble states alternately, then moves stepwise with a unit step of 6.46 nm. Accordingly, processive motion is achieved in the system (movie S2, Supporting Information). Since the mass of the neck linker is greater than that of other molecules, the motion of the neck linker is relatively slow. Besides, the neck linker is usually located between motors in the x-direction. Our simulation indicates that

a big mass that is less influenced by thermal fluctuation can be carried under this mechanism.

Similar to the single-headed motor system, E_{in} increases when the motor is subject to the liquid state. Kinesin can walk on a microtubule in one direction due to the low probability of backward steps.[10,12] Our simulation of motor "walking" behavior is consistent with the behavior of kinesin. As can be seen in Figure 7b, our motor moves processively in a fashion of combined hand-over-hand (8.0–8.15 μs and 8.4–8.5 μs) and inchworm models (8.3–8.4 μs). Apparently, this result seems inconsistent with some previous experiments.[12,28] We will discuss this issue below.

We also perform simulations with several different average lifetimes, τ = 8.8, 13.2, 17.6, 22.0, and 26.4 ns. In these simulations, we record the time to locate each motor before the other motor. This time divided by the total computing time is defined as $P(X_m)$ (summarized in Table 2). In the inchworm model, one head always leads, whereas in the hand-over-hand model, the two heads lead alternately. We distinguish the hand-over-hand and inchworm processive movements via direct observation. The hand-over-hand movement is defined as the stepping motion in which one motor proceeds two-unit lengths of the rail pattern (~13 nm) per single ATP cycle and overlaps the position of the other motor by that step. Other movement, for example, step by step, is viewed as the inchworm movement. In Table 2, N_{iw} and N_{hh} stand for the number of inchworm steps and the number of hand-over-hand steps, respectively. Compared with $P(X_{right})$ and $P(X_{left})$, the ratio is nearly the same, independent of τ, although the inchworm model is dominant. As previously described, our motor moves in a fashion of combined hand-over-hand and inchworm movements. The hand-over-hand step often occurs during processive movement. Consequently, $P(X_m)$s become nearly the same.
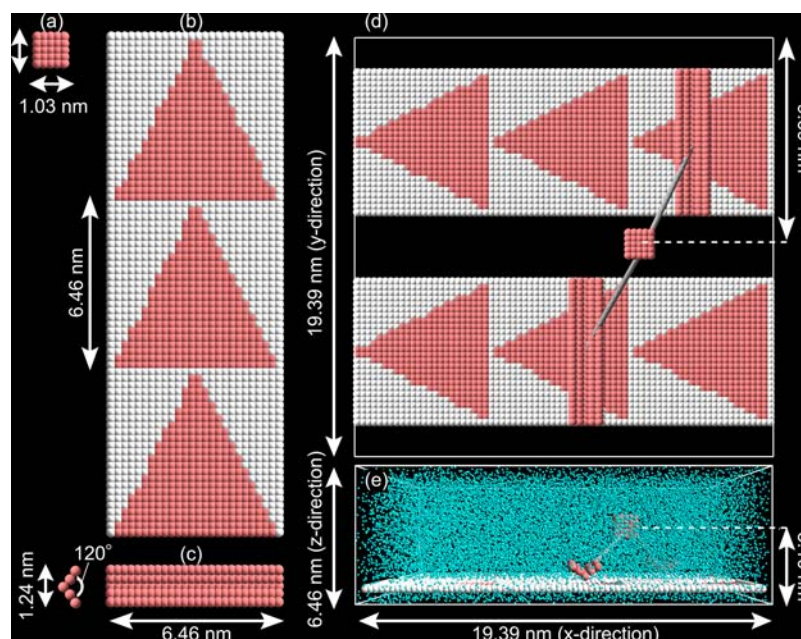
Figure 6. Double-headed motor system composed of a neck linker, two motors and two rails. Neck linker (a) is a block made of strongly hydrophobic particles (red). Rail (b) and motor (c) are same as single-headed motor system, respectively. Double-headed motor system in the x-y plane view (d), and in the x-z plane view (e). There are two motors on each rail. The motor is connected to the neck linker by a weak spring (gray bar in (d)). The kinesin model (red) and rail (red and white) are dipped in water.
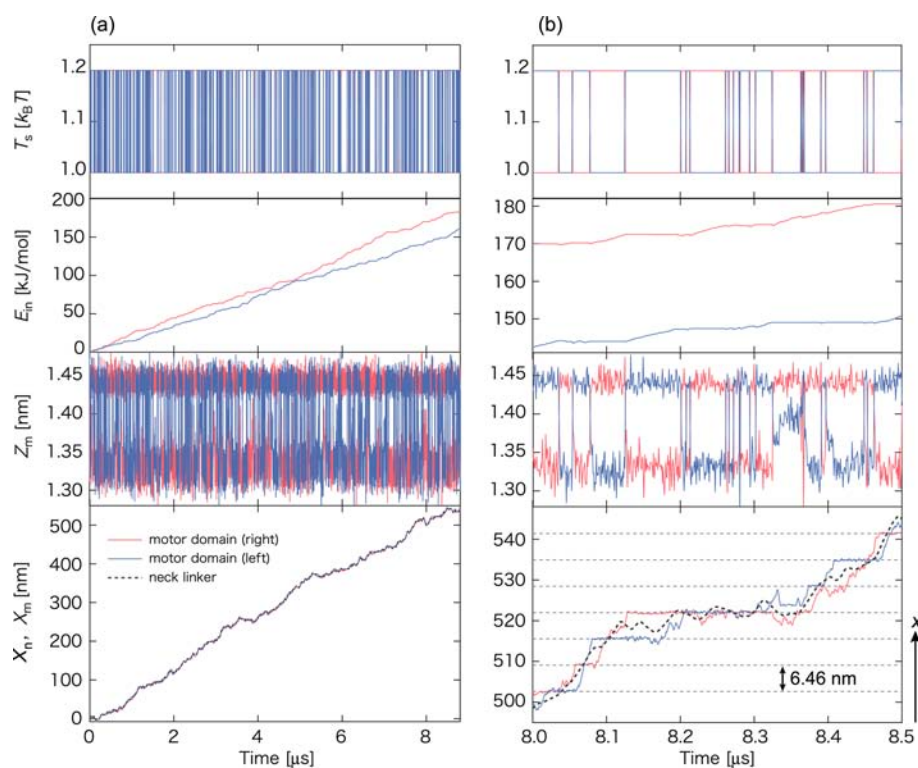

Figure 7. (a) Time evolution of the preset temperature of the motor, T_s, the input energy, E_{in}, the coordinates of the motor, Z_m and X_m, and the coordinate of the neck linker, X_n. (b) Zoomed-in view of panel a from 8.0 to 8.5 μs. The red, blue, and black dashed lines represent the right motor, the left motor, and the neck linker, respectively. Each motor can be transformed from the bubble state to the liquid state by supplying certain energy (top and middle panels). The motor "walks" in a fashion of combined inchworm model and hand-over-hand model.

As τ increases, the total number of steps decreases, and the fraction of hand-over-hand steps increases (Table 2). According to the experimental results reported by Yildiz et al., kinesin moves processively via the hand-over-hand mechanism, but not the inchworm mechanism. Our model differs from this experimental data in this aspect. However, the time for a single step that corresponds to an ATP cycle time is on the time scale of seconds in the actual kinesin motor protein, whereas that for our motor system is on the time scale of nanoseconds. Therefore, the ratio of the hand-over-hand step would be very high if τ is set on the order of seconds.

Table 2. Summary of the Numerical Results for Various Average Life Time, τ, Simulations

τ [ns]	$P(X_{\text{right}})$ [%]	$P(X_{\text{left}})$ [%]	N_{iw}	N_{hh}
8.8	48.4	51.6	395	11
13.2	50.1	49.9	356	18
17.6	49.8	50.2	309	33
22.0	48.6	51.4	274	36
26.4	50.9	49.1	257	43

Lastly, we show the time variation for the motion (in the x-direction) of single- and double-headed motor models with different negative external forces, F_{ext} (Figure 8). External forces
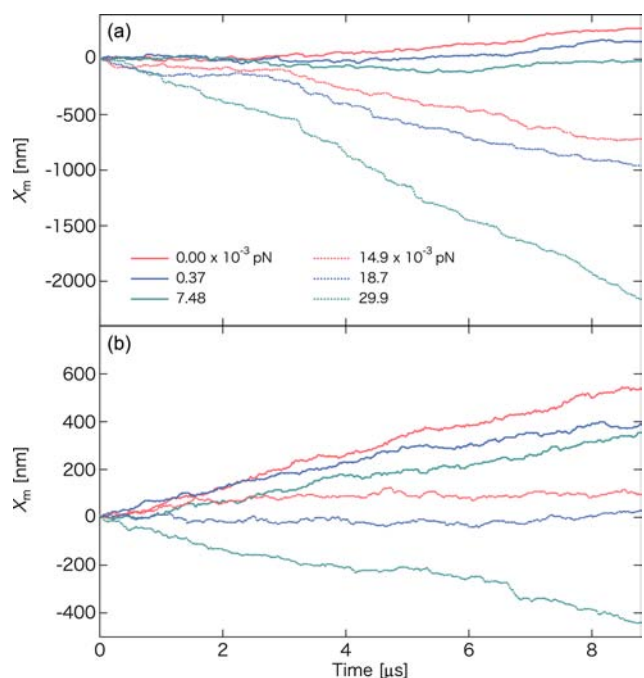

Figure 8. The coordinate of the motor in the x-direction, X_{m}, as a function of time under different magnitudes for the negative external force: (a) single-headed motor system and (b) double-headed motor system.

act on the motor in the single-headed motor model or on the neck linker in the double-headed motor model in the negative x-direction, and the magnitude of the force is set to be (0.37, 7.48, 14.9, 18.7, and 29.9) $\times 10^{-3}$ pN. Under the weak force ($F_{\text{ext}} < 0.37 \times 10^{-3}$ pN), both motor systems exhibit processive movements. As F_{ext} increases ($F_{\text{ext}} > 7.48 \times 10^{-3}$ pN), although the double-headed motor can move in one direction, the movement of motors is in the negative x-direction in the single-headed system due to increased backward steps, even with the same magnitude of the external force. The double-headed motor system involves two motors. Either motor can bind to the rail tightly in the bubble state. In other words, the motor in the bubble state plays the roll of an anchor with the rail. Thus, the double-headed motor can move processively under relatively strong external force. Under the greater force ($F_{\text{ext}} > 29.9 \times 10^{-3}$ pN), both systems exhibit backward movement. The frequency of backward steps for the single-headed motor system is higher than that for the double-headed motor system. Carter and Cros,[31] based on their experiment, suggested that the motor walks sustainably backward in ATP-dependent backward processivity under a very high backward load (above the stall

force). Similar motion behavior has been observed under high external force.

CONCLUSION

We devised two new motor systems driven by bubble formation in a hydrophobic channel. Our motor models are based on the notion of the "asymmetric Brownian ratchet model". The underlying switching mechanism is based on the phase transition between the bubble and liquid states due to the change of hydrophobic/hydrophilic parameter of the motor controlled by the temperature of the motor itself. This mechanism requires only the control of the hydrophobicity of the motor. It can be made to "walk" with high efficiency, depending on the material used for the motor. Moreover, we have measured the deviation of the stepping size and stepping time for motor systems that have several average life times. The distribution of stepping size was similar to the Gaussian distribution in the liquid states, whereas that in the bubble state is asymmetric for all τ values. The new motor models can provide a simulation guide to the design of biomimetic nanomachines. In addition, our motor systems are so small that may be massively packed akin to an integrated circuit. Such motor systems are also applicable to micromachine elements, which are typically required to operate continuously.

ASSOCIATED CONTENT

Ⓢ Supporting Information

Movie S1 showing the motor motion in single-headed motor system from 7.04 to 7.75 μs (the bubble formation is controlled by changing the hydrophobic feature of the motor; when the motor is hydrophobic, it is colored in red, and when it is hydrophilic, it is colored in blue; water particles just around the motor are displayed; the bubble state in the channel corresponds to the asymmetric potential state, and the liquid state in the channel corresponds to the random Brownian state for Feynman's asymmetric Brownian motor) and movie S2 showing the motor motion in in double-headed motor system from 8.0 to 8.5 μs (in this system, two motors are connected to the neck linker by a weak spring; when the motor is hydrophobic, it is colored in red, and when it is hydrophilic, it is colored in blue; water particles just around the motor are displayed; the hydrophobic feature of motors alternates; as a result, the double-headed motor model moves by a hand-over-hand mechanism along rails). This material is available free of charge via the Internet at http://pubs.acs.org.

AUTHOR INFORMATION

Corresponding Author
arai@mce.uec.ac.jp
Notes
The authors declare no competing financial interest.

ACKNOWLEDGMENTS

REFERENCES

(1) Feynman, R. P.; Leighton, R. B.and Sands, M. *Feynman Lectures on Physics*; Addison-Wesley: Reading, MA, 1963; Vol. *1*, Chapter 46.
(2) Córdova, N. J.; Ermentrout, B.; Oster, G. F. *Proc. Natl. Acad. Sci. U.S.A.* 1992, *89*, 339−343.

(3) Magnasco, M. O. *Phys. Rev. Lett.* **1993**, *71*, 1477−1481.

(4) Astumian, R. D.; Bier, M. *Phys. Rev. Lett.* **1994**, *72*, 1766−1769.

(5) Doering, C. R.; Horsthemke, W.; Riordan, J. *Phys. Rev. Lett.* **1994**, *72*, 2984−2987.

(6) Prost, J.; Chauwin, J. F.; Peliti, L.; Ajdari, A. *Phys. Rev. Lett.* **1994**, *72*, 2652−2655.

(7) Rousselet, J.; Salome, L.; Ajdari, A.; Prost, J. *Nature* **1994**, *370*, 446−448.

(8) Astumian, R. D. *Sci. Am.* **2001**, *285*, 56−64.

(9) Kay, E. R.; Leigh, D. A.; Zerbetto, F. *Angew. Chem., Int. Ed.* **2007**, *46*, 72−191.

(10) Okada, Y.; Hirokawa, N. *Science* **1999**, *283*, 1152−1157.

(11) Tomishige, M.; Klopfenstein, D. R.; Vale, R. D. *Science* **2002**, *297*, 2263−2267.

(12) Okada, Y.; Higuchi, H.; Hirokawa, N. *Nature* **2003**, *424*, 574−577.

(13) Okada, Y.; Hirokawa, N. *Proc. Natl. Acad. Sci. U.S.A.* **2000**, *97*, 640−645.

(14) Hirokawa, N.; Nitta, R.; Okada, Y. *Nat. Rev.* **2009**, *10*, 877−884.

(15) Yanagida, T.; Arata, T.; Oosawa, F. *Nature* **1985**, *316*, 366−369.

(16) Arai, N.; Yasuoka, K.; Koishi, T.; Ebisuzaki, T. *ACS Nano* **2010**, *4*, 5905−5913.

(17) Ueki, T.; Watanabe, M. *Chem. Lett.* **2006**, *35*, 964−965.

(18) Seuring, J.; Bayer, F. M.; Huber, K.; Agarwal, S. *Macromolecules* **2012**, *45*, 374−384.

(19) Hoogerbrugge, P. J.; Koleman, J. M. V. A. *Europhys. Lett.* **1992**, *19*, 155−160.

(20) Espanõl, P.; Warren, P. B. *Europhys. Lett.* **1995**, *30*, 191−196.

(21) Groot, R. D.; Warren, P. B. *J. Chem. Phys.* **1997**, *107*, 4423−4435.

(22) Yang, K.; Ma, Y.-Q. *Nat. Nanotechnol.* **2010**, *5*, 579−583.

(23) Arai, N.; Yasuoka, K.; Zeng, X. C. *J. Am. Chem. Soc.* **2008**, *130*, 7916−7920.

(24) Arai, N.; Yasuoka, K.; Zeng, X. C. *Langmuir* **2012**, *28*, 2866−2872.

(25) Park, S. Y.; Lytton-Jean, A. K. R.; Lee, B.; Weigand, S.; Schatz, G. C.; Mirkin, C. A. *Nature* **2008**, *451*, 553−556.

(26) Cigler, P.; Lytton-Jean, A. K. R.; Anderson, D. G.; Finn, M. G.; Park, S. Y. *Nat. Mater.* **2010**, *9*, 918−922.

(27) Groot, R. D.; Rabone, K. L. *Biophys. J.* **2010**, *81*, 725−736.

(28) Yildiz, A.; Tomishige, M.; Vale, R. D.; Selvin, P. R. *Science* **2004**, *303*, 676−678.

(29) Yildiz, A.; Tomishige, M.; Gennerich, A.; Vale, R. D. *Cell* **2008**, *134*, 1030−1041.

(30) Berg, J. M.; Tymoczko, J. L.; Stryer, L. *Biochemistry*, 5th ed.; W H Freeman & Co: New York, 2002; Chapter 34.

(31) Carter, N. J.; Cross, R. A. *Nature* **2005**, *435*, 308−312.